Positive mass balance during the late 20th century on Austfonna, Svalbard revealed using satellite radar interferometry

S. Bevan, A. Luckman and T. Murray

Glaciology Group,

School of the Environment and Society,

University of Wales Swansea

June 13, 2006

Abstract

Determining whether increasing temperature or precipitation will dominate the cryospheric response to climate change is key to forecasting future sea-level rise. The volume of ice contained in the ice caps and glaciers of the Arctic archipelago of Svalbard is small compared with that of the Greenland or Antarctic ice sheets, but is likely to be affected much more rapidly in the short term by climate change.

This study investigates the mass balance of Austfonna, Svalbard's largest ice

cap. Equilibrium-line fluxes for the whole ice cap, and for individual drainage basins, were estimated by combining surface velocities measured using satellite radar interferometry with ice thicknesses derived from radio echo sounding. These fluxes were compared with balance fluxes to reveal that during the 1990's the total mass balance of the accumulation zone was $5.6 \pm 2 \times 10^8$ m^3a^{-1}. Three basins in the quiescent phase of their surge cycles contributed 75% of this accumulation. The remaining signal may be attributable either to as yet unidentified surge-type glaciers, or to increased precipitation. This result emphasises the importance of considering the surge dynamics of glaciers when attempting to draw any conclusions on climate change based on snapshot observations of the cryosphere.

Introduction

Recent changes in atmospheric circulation have resulted in a 0.5 °C per decade increase in the recorded annual mean air temperature at Longyearbyen on Spitsbergen, western Svalbard, and a precipitation increase of 1.7% per decade, since the late 1960s (Førland and Hanssen-Bauer, 2002). These data are supported by ice-core analyses from the ice cap Lomonosovfonna, the highest ice field on Spitsbergen, which indicated an accumulation rate increase of 25% over the latter half of the 20th century compared with the years from 1715 to 1950 (Pohjola and others, 2002).

Observations suggest that most low-altitude Arctic glaciers have been re-

treating since the 1920s, but with no significant increase in melting over the last 40 years (McCarthy and others, 2001). On Svalbard, ice masses are known to have generally retreated since the Holocene (Hagen and Liestøl, 1990). However, the present day mass balance of the majority of Svalbard's ice caps and glaciers is poorly defined so the contempory response to recent climate change is difficult to assess. In-situ mass-balance observations are mostly limited to a small number of more easily accessible glaciers in western Spitsbergen. However, the present climate on Svalbard is determined by a balance between two weather regimes; the first characterised by frequent passages of low-pressure systems from the south-west, and the second bringing the snow-bearing cold north-easterly polar winds from the Barents Sea. This zonal climate variation means that mass-balance measurements on Spitsbergen are probably not representative of the climate of ice masses to the east of Svalbard, such as Austfonna (8120 km^2) and Vestfonna (2510 km^2), the two largest ice caps.

An estimate of the overall net balance of Svalbard ice masses of -4.5 km^3a^{-1} has been made by combining net balance altitude gradients for 13 different regions in Svalbard with a digital elevation model (Hagen and others, 2003). Austfonna was included in this net balance estimate, and was determined to have a net balance close to zero using a balance ratio chosen to match that of other areas in Svalbard due to the lack of information on ablation rates.

In this study we estimate the total mass balance for the accumulation zone of Austfonna by calculating the difference between measured and balance fluxes across the equilibrium line. The measured fluxes were the product of remotely

sensed surface velocities and radio-echo sounded ice thicknesses. The balance fluxes were based on a specific mass balance distribution, derived from ice-core data, integrated over the accumulation area. When referring to mass balance the terminology of Bamber and Payne (2004) is used. This terminology defines specific mass balance to include only the sum of local accumulation and ablation; and local mass balance is used to describe the local mass change of the column. In order to obtain a picture of the spatial distribution of local mass balance, flux differences were apportioned according to drainage basin. Dividing each basin flux difference by the area of its accumulation zone gave a basin-mean local mass balance.

Methodology and data

Calculation of balance fluxes

The balance flux is defined as the rate at which ice must be transported downstream in order to be in equilibrium with the accumulation and ablation rates and hence preserve a stable surface profile. The mean annual balance flux at the ELA, for the whole ice cap and for individual drainage basin areas (S_c), was calculated by integrating the distribution of mean annual specific mass balance (B_n):

$$F_\mathrm{b} = \int_{S_\mathrm{c}} B_\mathrm{n} \mathrm{d}S. \tag{1}$$

Drainage basin boundaries were geocoded and digitised from a glacier inventory of Svalbard (Hagen and others, 1993), and are referenced according to the World

Glacier Inventory identification system.

The distribution of mean annual specific mass balance (B_n) was based on a set of transects of shallow ice cores drilled in 1997/98 in which the 1986 Chernobyl nuclear accident radioactive reference horizon could be detected (Pinglot and others, 2001). It has been shown that estimates of specific balance based on core data correlate well with direct measurements (Lefauconnier and others, 1994). In order to calculate the B_n distribution, altitude gradients of B_n and estimates of the ELA based on the cores (Pinglot and others, 2001) were extrapolated over a 100 m resolution grid using the Generic Mapping Tools minimum curvature spline interpolator with a tension of 0.65. The altitude gradients of B_n were then multiplied by the height above ELA, using elevations from a 100 m resolution digital elevation model (DEM) supplied by the Norsk Polarinstitutt. This DEM was used rather than the interferometric heights calculated as part of the surface velocity method, in order to maintain independence between the two flux estimates.

Estimation of downslope velocity

The procedures for deriving glacier surface velocities using synthetic aperture radar interferometry (SRI) are well established (Kwok and Fahnestock, 1996). In this study differential SRI was carried out on pairs of 3-day ERS-1 interferograms from 1994 and 1-day ERS-1/ERS-2 interferograms from 1996 (see Table 1 and Figure 1), using Gamma Remote Sensing software. In brief, pairs of interferograms were differenced to remove the effects of surface displacement

on interferometric phase, leaving only topographic phase effects. After appropriate scaling, this topographic phase could then be removed from one of the original interferograms. The resulting unwrapped interferograms then provided measurements of surface displacement in the line-of-sight (LOS) direction of the radar, over the time period spanned by each interferogram.

Three-dimensional surface velocities were derived from these LOS surface displacements by making the assumption that the ice flows parallel to the surface (Kwok and Fahnestock, 1996), and in the direction of maximum surface slope (Paterson, 1994; Unwin, 1998). The surface elevation used to compute flow directions was generated during the first part of the differential procedure by using a number of ground control points (GCPs) to create a DEM from the topographic phase. Some GCPs were provided by assigning the coast, as identified on the multilooked synthetic aperture radar (SAR) intensity images, to a height of 0 m a.s.l. On the ice cap, 650 GCPs were taken from 1996 NASA airborne laser altimetry data (shown in Figure 1; Bamber, personal communication 2005). In order to determine flow directions the DEM was not required to be of absolute accuracy. Differences between the effective heights of the scattering layers between lidar and the C-band radar, which may penetrate up to 9 ± 2 m in cold polar firn (Rignot and others, 2001) are not, therefore, important.

In order to obtain as complete a coverage as possible over the ice cap, a composite of surface velocities was produced by infilling the 1996 results with measurements from 1994. Surface velocities were occasionally retrievable for the same area from more than one interferometric dataset. This overlap enabled us

to ascertain that surface velocities had not changed significantly over this period, as changing the order of priority of datasets when producing the composite made no discernible difference to the resulting flux estimates.

The spatial resolution of the SAR data is $\sim$ 4 m in the azimuth direction and $\sim$ 20 m in the ground-range direction. After multilooking to reduce phase noise and conversion to a geographic co-ordinate system the spatial resolution of the 3D velocities was 50 m$\times$50 m. A profile of annual surface displacements in the downslope direction was extracted along the equilibrium line at intervals of 50 m for use in the flux calculations.

Calculation of measured fluxes

Measured fluxes in m^3 of water equivalent per annum (m^3weq. a^{-1}) were computed by multiplying the equilibrium-line profile of annual surface displacements by the product of the extraction interval and the ice thickness at that point, using a factor of 0.84 to allow for the relative density of ice to water (Paterson, 1994).

The ice thickness distribution was constructed from airborne radio echo sounding (RES) data collected in 1983 (Dowdeswell and others, 1986) with the additional constraint of ice margins, which may be grounded below sea level, being set to a thickness of 100 m as it has been observed that the ice is generally at least this thick even at the ice-cap margins (Dowdeswell and others, 1986). The 50 m wide flux elements along the equilibrium line were then summed for each drainage basin and for the entire accumulation zone.

Error assessment

The errors are discussed according to those which affect the velocity measurements, the annual flux estimates, and the balance fluxes. Estimates of annual flux were obtained by combining measured surface velocities with ice thicknesses assuming that sliding was the primary cause of ice transport and that the measured velocities were representative of mean annual velocities. The possible consequences of incorrectly assuming sliding, and of seasonal velocity variations, are considered and quantified in the Discussion section.

Interferometric velocities

Errors in measured velocities can be separated into those incurred in producing satellite LOS velocities and those arising on resolving three-dimensional (3D) velocities. The largest probable sources of error in calculating the LOS velocities are atmospheric path-length distortions and baseline errors (Mohr and others, 2003), the effect of interferometric phase noise is also considered.

For differential interferometry, the sensitivity of LOS velocity estimates to atmospheric path-length changes depends on the baselines and time spans of the constituent interferograms (Mohr and others, 2003). In the dry polar atmosphere, root mean square (r.m.s.) variations in atmospheric path length are likely to be less than 0.3 cm (Mohr and others, 2003). According to the sensitivities to change in atmospheric path length for the differential image pairs used in this study (see Table 1) the resulting velocity errors will be less than 1 ma^{-1}.

Inaccuracies in baselines can cause errors in LOS velocities when the topographic phase effects are removed. Line-of-sight velocity errors based on the standard deviation of the phase-scaling fit function used to scale the topography-only to the velocity-pair interferograms were less than 2 ma^{-1}.

Phase noise introduces an effective path-length error which impacts on velocity measurements in the same way as atmospheric path-length changes (Mohr and others, 2003). In this study the errors in velocity at the ELA resulting from phase noise were estimated to be less than 0.5 ma^{-1}.

Errors arising from the conversion of LOS velocities to 3D velocities are amplified as the angle between flow direction and satellite look direction increases (Fatland and Lingle, 1998). In this study surface displacements were not calculated where downslope directions were more than 65° from the satellite LOS direction. The use of a composite map of surface displacements generated from ascending and descending satellite trajectory azimuths minimised the area lost by this flow-azimuth cut-off. The errors introduced by assuming downslope flow were estimated empirically, where possible, by using a 'dual-azimuth' technique (Joughin and others, 1998; Luckman and others, 2002) to measure velocities. Along the equilibrium line the r.m.s. difference between dual-azimuth and downslope velocities was less than 6 ma^{-1}.

In summary, assuming the sources of error to be independent from one another, total theoretical errors in LOS velocity measurements of less than ± 3 ma^{-1}, combined with the errors produced as a result of assuming a flow direction lead to an overall 3D velocity error of less than ± 7 ma^{-1}.

Errors in measured flux

Accurate flux estimates also depend on accurate ice-thickness measurements. The ice thicknesses used in this study were estimated to have an accuracy of ±6% (Dowdeswell and others, 1986). Making allowance for errors arising as a result of interpolation and extrapolation, ice thicknesses used in the flux calculations are likely to have an accuracy of ±10%. Any changes in ice thickness between the dates of the RES survey and the velocity measurements will probably be within this ±10%.

In combining errors in displacement and ice thickness to estimate errors in flux for a particular drainage basin it was recognised that neither source of error is likely to be independent from one 50 m flux element to another. Therefore, the errors in measured basin fluxes were calculated from the sum of individual flux element errors. It was assumed, however, that errors were not correlated from basin to basin when calculating the probable error in flux for the ice cap as a whole.

Errors in balance flux

The mean annual specific mass balance measurements based on the ice cores were estimated to be accurate to within ±10% (Pinglot and others, 2001). In this study the estimated total accumulation for the entire accumulation zone of Austfonna was $10.5 \times 10^8 \mathrm{m}^3\mathrm{a}^{-1}$; the equivalent figure as calculated by Pinglot and others (2001) was $9.8 \times 10^8 \mathrm{m}^3\mathrm{a}^{-1}$. Basin and total accumulation rates in this study are therefore estimated to have an accuracy of about ±10%.

Results

Balance fluxes

Based on the ice-core data, specific mass balances within the accumulation zone of Austfonna reach a maximum of 0.45 mweq.a^{-1} toward the summit of the ice cap at an altitude of ∼800 m. Integrating the specific mass balance distribution over the 5700 km^2 accumulation zone of Austfonna results in an estimated equilibrium-line balance flux of 10.5×10^8 m^{3}weq.a^{-1}. Basin equilibrium-line balance fluxes varied from 1.9×10^8 m^{3}weq.a^{-1} for basin 21108, down to 8.0×10^4 m^{3}weq.a^{-1} for basin 25203, the variations being due to the altitude and areas of the different catchments (see Figure 3 for basin locations).

Measured velocities and fluxes

Downslope SRI velocities were obtained over almost all of Austfonna, Vestfonna, and the two smaller ice caps to the south-west of Austfonna (Figure 2). Outlet glaciers with maximum velocities of up to 100–150 ma^{-1} can be identified at various points around the ice cap. Ice divides are characterised by low velocities. Austfonna's ELA as extrapolated from the ice-core estimates, and along which the measured velocities and ice thicknesses were extracted, varies from just over 100 m in the south-east to over 460 m in the north-east (black contour on Figure 2). The ice thickness reaches a maximum of ∼590 m toward the centre of the ice cap, and for most of the north and east coasts the ice is grounded below sea level. Along the equilibrium line the ice thickness is 300–400 m in the north and ∼100 m in the south.

The total measured ELA flux for Austfonna was $4.9 \pm 1.0 \times 10^8$ m^3weq.a^{-1}. Breaking the flux down into individual drainage basins, the largest contributions were 1.1×10^8 m^3weq.a^{-1} from basin 21106, and 0.7×10^8 m^3weq.a^{-1} from basins 21108 and 25204, with estimated errors of about $\pm 0.3 \times 10^8$ m^3weq.a^{-1}.

Mass balance of the ice cap

The total mass balance of the ice cap, i.e., the difference between the measured and balance fluxes, was found to be of the order of $5.6 \pm 2.0 \times 10^8 m^3$weq.$a^{-1}$. Using the basin boundaries it was possible to apportion this flux imbalance according to drainage basin. The most positive total mass balance was 1.9×10^8 m^3weq.a^{-1} for basin 21108, with a further 1.1×10^8 m^3weq.a^{-1} and 1.2×10^8 m^3weq.a^{-1} for basins 21110 and 22203, respectively.

The mean local mass balances, in mweq.a^{-1}, represent the difference between balance and measured fluxes divided by the area of the accumulation zone for each basin (see Figure 3). The most positive mean local mass balances found were for basins 22203, 22204 and 21108 with 0.23, 0.20 and 0.18 mweq.a^{-1}, respectively. The most negative local mass balances was -0.22 mweq.a^{-1} for basin 22202.

Residence times

Another parameter derived from the data available here was the approximate residence time for each drainage basin. The residence time is simply the total volume of ice contained within the accumulation zone of each basin divided by the flux rate at the equilibrium line. Across Austfonna values range from around

500 years for the smaller glaciers to over 10,000 years for the larger slow-flowing glaciers.

Discussion

The total mass balance of the accumulation zone of Austfonna was found to be $5.6 \pm 2.0 \times 10^8$ $m^3 weq.a^{-1}$. This figure represents just over half the annual accumulation of the ice cap and would seem to indicate that recent accumulation increases are leading to a steady gain in mass of the ice cap. However, when the spatial distribution of total mass balance over the ice cap is analysed it becomes obvious that the imbalance between balance and measured fluxes is far from uniform. About 75% of the positive total mass balance comes from just three basins, 21108, 21110 and 22203, all of which are known to be surge-type glaciers in their quiescent phases.

Basin 21108, was shown to have been in surge in 1992, but to have slowed down by 1994 (Dowdeswell and others, 1999). By 1996 it is shown here to have a mean local mass balance of 0.18 $mweq.a^{-1}$, and therefore continuing to recover its pre-surge profile. Between 1936 and 1938 basin 21110, named Bråsvellbreen, underwent the largest surge known for any ice mass (Drewry and Liestøl, 1985), the 30 km long ice edge advanced by 2 km, 60 years later it is still accumulating mass. Basin 22203, Etonbreen, also surged in 1938.

The local mass-balance distribution suggests that other basins, notably 22204 (Winsnesbreen) and 25105, may also be accumulating mass prior to a surge. Neither of these basins show signs of ever having surged, nor have they been

identified as surge-type glaciers on the basis of driving stresses (Dowdeswell, 1986), or glacier length and substrate (Jiskoot and others, 2000). Basin 25204, Leighbreen, was identified by Dowdeswell (1986) as possibly being of surge type on the basis of its low driving stresses and surface profile. Measured velocities, deriving from 1994 data, were below 40 m a^{-1} at all points on this glacier and showed no acceleration relative to 1992 velocities. Hence, although its local mass balance was negative in 1994, flow rates do not suggest that it was in surge.

In measuring the equilibrium fluxes this study made two assumptions referred to, but not quantified in the error analysis. The first was that all of the ice transport was achieved by basal sliding rather than by ice deformation, and the second was that the velocities measured are representative of annual velocities.

It is probable that for some sections of the equilibrium line the first assumption does not hold true, and that by assuming sliding the flux is being overestimated by up to 20% (Paterson, 1994). This is only likely to be the case in areas of low flux, as it has been estimated that for much of Austfonna the maximum flow rate that can be achieved by deformation alone is 5 ma^{-1} (Dowdeswell and others, 1999), and it is apparent that at the ELA most surface velocities exceed this. In addition, plumes of sediment-laden basal meltwater have been identified in Landsat images for a number of tidewater-terminating glaciers along the eastern edge of Austfonna indicating that their bases are at pressure melting point and hence sliding is likely (Dowdeswell and Drewry,

1989). Of the individual basins where a negative total mass balance is indicated, only basin 21106 would be tipped into a positive balance by a basin-wide 20% decrease in flux.

If the second assumption did not hold true it may be expected to have the opposite effect, i.e. late winter or early spring flux rates measured here might underestimate mean annual flux rates and hence result in an overestimate of total mass balance. In order for the total mass balance for the ice cap to be zero, the mean annual velocities at all points around the equilibrium line would have to be double those measured. This ratio of mean annual to spring velocities would be far in excess of the seasonal variations generally observed on other polythermal Arctic glaciers, for example, on Hessbreen, Spitsbergen (Sund and Eiken, 2004), Storglaciaren, Sweden (Hooke and others, 1983), or Jakobshavn Isbrae, Greenland (Luckman and Murray, 2005). Kongsvegen (Melvold and Hagen, 1998) and Finsterwalderbreen (Nuttall and others, 1997) on Spitsbergen have both been observed to have summer surface velocities double those of winter at upper levels. However, this seasonal velocity increase translates into a mean-annual to spring flux rate ratio of 1.5 because of the relative number of months over which the velocitites were measured.

Evidence in support of continuing increases in total mass balance of the ice cap comes from repeat-pass airborne laser altimetry surveys in 1996 and 2002 (Bamber and others, 2004), the surface elevations acquired in 1996 being those used as ground control for the interferometry in this study and shown in Figure 1. The results of the surveys indicated that from 1996 to 2002 ice-

surface elevations over central regions of the ice cap increased by an average of 0.5 ma^{-1}. Even allowing for the conversion from ice to water equivalent, this value is twice as large as the largest mean local mass balance calculated here.

Bamber and others (2004) concluded that the elevation increases (dh/dt) detected by the laser altimetry surveys were not dynamic in origin but were due to increased accumulation rates. This conclusion was reached partly on the basis that the increases spanned several dynamically independent drainage basins. For example, there was no change in dh/dt crossing from basin 21108 to 22203 (referred to as basins 3 and 17, respectively, in Bamber and others (2004)). Our study indicates that although these two basins surged some 55 years apart their accumulation zones are, in fact, exhibiting very similar mean local mass balances. The elevation increase detected by the altimetry survey appears to decrease markedly from basin 21108 into basins 21106 and 25204, coinciding with the change from positive to negative mean local mass balances detected here. The measured dh/dt's mostly post-date the ice-core accumulation rate estimates which showed no signs of temporal trend between 1963–86 and 1986–98 (Pinglot and others, 2001). Therefore, we propose that the extensive elevation increases detected by the laser altimetry survey may be the result both of ongoing basin dynamics and a recent increase in accumulation rate.

In interpreting any imbalance between balance and measured fluxes in terms of mass gain of the ice cap it is important to note that a comparison is being made here between quantities that are representative of different time scales. The balance fluxes, being based on ice cores, are a mean over more than a

decade and hence can be taken to represent current climate. The measured fluxes are only a contemporary snapshot but, for steady-flow glaciers, are in fact a reflection of past climatic conditions because of the long dynamic response time of Arctic ice masses. An order-of-magnitude estimate of the response time for Austfonna, given by the ratio of the maximum ice thickness to the ablation rate at the terminus (Paterson, 1994), is 1000 years. Alternatively, relative response times of individual drainage basins can be inferred from the residence times which were all in excess of 500 years.

It is also important to emphasise that this analysis deals only with the accumulation zone of Austfonna. In order for the mass balance of the ice cap to be interpreted in terms of its impact on global sea levels ablation rates and calving fluxes must also be considered. It may be possible to use remote-sensing methods to estimate calving fluxes, but at present there is very little information available on ablation rates for Austfonna.

Conclusions

Although predictions and observations in the Arctic indicate that Svalbard's ice caps will be important indicators of climate change, mass-balance assessments of glaciers in Svalbard are very limited. This study aimed to compare measured and balance fluxes at the ELA on Austfonna, and showed that during the period 1994–96 the accumulation zone was in a state of positive mass balance. Measured surface velocities obtained using SRI combined with RES ice thicknesses gave an equilibrium-line annual flux of $4.9 \pm 1.0 \times 10^8$ $m^3 weq.a^{-1}$; equivalent

to about half the total annual accumulation. The spatial distribution of local mass balance was revealed by separately analysing each drainage basin. This analysis showed the positive mass balance to be contributed mainly by three glaciers known to be in surge recovery. The mean local mass balance within these basins is not inconsistent with elevation changes for 1996 to 2002 measured using repeat laser altimetry surveys, but indicates an underlying dynamic component to the changes.

Acknowledgments

The 1996 ERS SAR images were supplied by ESA under the VECTRA project AO108, coordinated by Andrew Shepherd. We are also grateful to Tazio Strozzi of Gamma Remote Sensing who made available the 1994 images, also acquired under VECTRA. Thanks are due to the Norsk Polarinstitutt who kindly supplied the 100 m resolution DEM, Jonathon Bamber for the 1996 airborne laser altimetry data, and to Helena Sykes who georeferenced the glacier inventory maps. Suzanne Bevan was funded by UK Natural Environment Research Council PhD Studentship NER/S/A/2003/11395.

References

Bamber, J., Krabill, W., Raper, V., and Dowdeswell, J., 2004, Anomalous recent growth of part of a large Arctic ice cap: Austfonna, Svalbard. *Geophys. Res. Lett.*, **31**, doi:10.1029/2004GL019667.

Bamber, J. L., and Payne, A. J., 2004, *Mass balance of the cryosphere.* (Cambridge University Press).

Dowdeswell, J. A., 1986, Drainage basin characteristics of Nordaustlandet ice caps, Svalbard. *J. Glaciol.*, **32**, 31–38.

Dowdeswell, J. A., and Drewry, D. J., 1989, The dynamics of Austfonna, Nordaustlandet, Svalbard: Surface velocities, mass balance, and subglacial meltwater. *Annals of Glaciology*, **12**, 37–45.

Dowdeswell, J. A., Drewry, D. J., Cooper, A. P. R., Gorman, M. R., Liestøl, O., and Orheim, O., 1986, Digital mapping of the Nordaustlandet ice caps from airborne geophysical investigations. *Annals of Glaciology*, **8**, 51–58.

Dowdeswell, J. A., Unwin, B., Nuttall, A.-M., and Wingham, D. J., 1999, Velocity structure, flow instability and mass flux on a large Artic ice cap from satellite radar interferometry. *Earth Planet. Sci. Lett.*, **167**, 131–140.

Drewry, D. J., and Liestøl, O., 1985, Glaciologcial investigations of surging ice caps in Nordaustlandet, Svalbard, 1983. *Polar Record*, **22**, 357–378.

Fatland, D. R., and Lingle, C. S., 1998, Analysis of the 1993–95 Bering Glacier (Alaska) surge using differential SAR interferometry. *J. Glaciol.*, **44**, 532–546.

Førland, E. J., and Hanssen-Bauer, I., 2002, Increased precipitation in the Norwegian Arctic: True or false? *Climate change*, **46**, 485–509.

Hagen, J. O., and Liestøl, O., 1990, Long-term glacier mass-balance investigations in Svalbard, 1950–88. *Annals of Glaciology*, **14**, 102–106.

Hagen, J. O., Liestol, O., Roland, E., and Jorgensen, T., 1993, *Glacier atlas of Svalbard and Jan Mayen* (Norsk Polar Institutt).

Hagen, J. O., Melvold, K., Pinglot, F., and Dowdeswell, J. A., 2003, On the net mass balance of the glaciers and ice caps in Svalbard, Nowegian Arctic. *Arct. Antarct. Alp. Res.*, **35, No.2**, 264–270.

Hooke, R. L., Brzozowski, J., and Bronge, C., 1983, Seasonal variations in surface velocity, Storglaciaren, Sweden. *Geogr. Ann.*, **65**, 263–277.

Jiskoot, H., Murray, T., and Boyle, P., 2000, Controls of the distribution of surge-type glaciers in Svalbard. *J. Glaciol.*, **154**, 412–422.

Joughin, I. R., Kwok, R., and Fahnestok, M. A., 1998, Interferometric estimation of three-dimensional ice-flow using ascending and descending passes. *IEEE Trans. Geosci. Remote Sensing*, **36**, 25–37.

Kwok, R., and Fahnestock, M. A., 1996, Ice sheet motion and topography from radar interferometry. *IEEE Trans. Geosci. Remote Sensing*, **34**, 189–200.

Lefauconnier, B., Hagen, J. O., Pinglot, J. F., and Pourchet, M., 1994, Mass-balance estimates on the glacier complex Kongsvegen and

Sveabreen, Spitsbergen, Svalbard, using radioactive layers. *J. Glaciol.*, **40**, 368–376.

Luckman, A., and Murray, T., 2005, Seasonal variations in velocity before retreat of Jakobshavn Isbrae, Greenland. *Geophys. Res. Lett.*, **32**, doi:10.1029/2005GL022519, 2005.

Luckman, A., Murray, T., and Strozzi, T., 2002, Surface flow evolution throughout a glacier surge measured by satellite radar interferometry. *Geophys. Res. Lett.*, **29**, doi: 10.1029/2001GL014570, 2002.

McCarthy, J. J., Canziani, O. F., Leary, N. A., Dokken, D. J., and White, K. S. (editors), 2001, *Climate Change 2001: Impacts, Adaptation, and Vulnerability. Report of IPCC Working Group II* (Cambridge University Press).

Melvold, K., and Hagen, J. O., 1998, Evolution of a surge-type glacier in its quiescent phase: Kongsvegen, Spitsbergen, 1964–95. *J. Glaciol.*, **44**, 394–404.

Mohr, J. J., Reeh, N., and Madsen, S. N., 2003, Accuracy of three-dimensional glacier surface velocities derived from radar interferometry and ice-sounding radar measurements. *J. Glaciol.*, **49**, 210–222.

Nuttall, A.-M., Hagen, J. O., and Dowdeswell, J., 1997, Quiescent-phase changes in velocity and geometry of Finsterwalderbreen, a surge-type glacier in Svalbard. *Annals of Glaciology*, **24**, 249–254.

Paterson, W. S. B., 1994, *The physics of glaciers*, third edition (Elsevier Science Ltd.).

Pinglot, J. F., Hagen, J. O., Melvold, K., Eiken, T., and Vincent, C., 2001, A mean net accumulation pattern derived from radioactive layers and radar soundings on Austfonna, Nordaustlandet, Svalbard. *J. Glaciol.*, **47**, 555–566.

Pohjola, V. A., Martma, T., Meijer, H. A. J., Moore, J. C., Isaksson, E., Vaikmäe, R., and van de Wal, R. S. W., 2002, Reconstruction of three centuries of annual accumulation rates based on the record of stable isotopes of water from Lomonosovfonna, Svalbard. *Annals of Glaciology*, **35**, 57–62.

Rignot, E., Echelmeyer, K., and Krabill, W., 2001, Penetraton depth of interferometric synthetic-aperture radar signals in snow and ice. *Geophys. Res. Lett.*, **28**, 3501–3504.

Sund, M., and Eiken, T., 2004, Quiescent phase dynamics and surge history of a polythermal glacier: Hessbreen, Svalbard. *J. Glaciol.*, **50**, 547–555.

Unwin, B. V., 1998, *Arctic ice cap velocity variations revealed using ERS SAR interferometry*, Ph.D. thesis, University College London.

Frame	Dates	ΔT	Baseline midscene	Sensitivity to path length distortion
1	05–06/03/96	1 day	180.9 m	3.1 $ma^{-1}cm^{-1}$
	09–10/04/96*	1 day	-32.6 m	
2	05–06/03/96	1 day	179.2 m	3.1 $ma^{-1}cm^{-1}$
	09–10/04/96*	1 day	-36.8 m	
3	06–09/01/94*	3 days	-67.4 m	0.9 $ma^{-1}cm^{-1}$
	09–12/01/94	3 days	80.9 m	
4	02–05/03/94*	3 days	-2.8 m	1.2 $ma^{-1}cm^{-1}$
	14–17/03/94	3 days	78.1 m	

Table 1: Interferogram pairs (see Figure 1 for locations) used for differential processing. Interferograms used for velocity calculations are indicated by '*'. ΔT is the time spanned by the interferogram. Locations of frame numbers are shown in Figure 1.

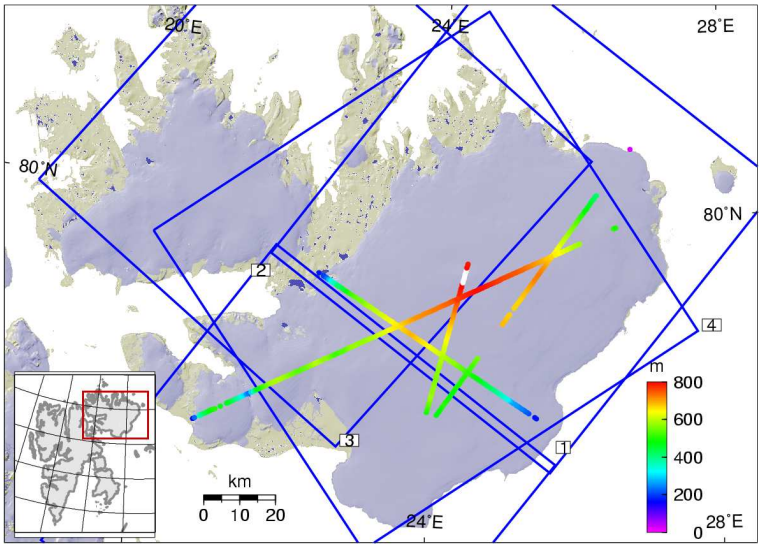

Figure 1: Airborne laser altimeter data points (Jonathon Bamber, personal communication), and location of data frames listed in Table 1. Inset shows location of Nordaustlandet within Svalbard.

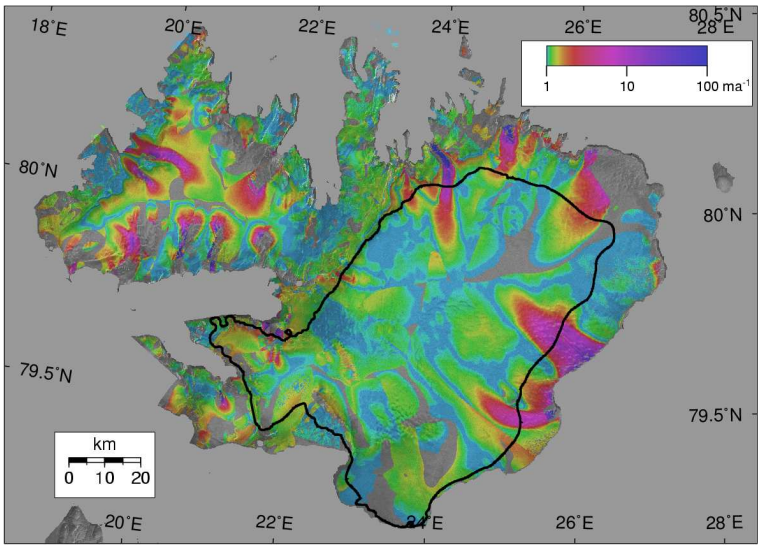

Figure 2: Composite of downslope interferometric velocities. In grey are regions for which it was not possible to retrieve velocities, using the data selected for this study, either due to phase coherence losses or flow-direction restrictions. The black line marks the equlibrium line altitude.

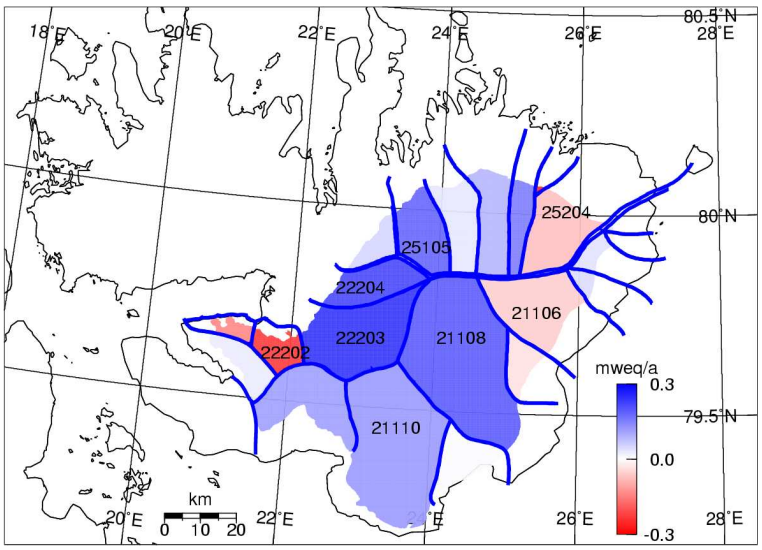

Figure 3: Basin-mean local mass balance. Shown in blue are those basins for which the mean local mass balance was positive, and in red those for which it was negative.